Progress in Organic Coatings 84 (2015) 42–49

Contents lists available at ScienceDirect

Progress in Organic Coatings

journal homepage: www.elsevier.com/locate/porgcoat

Preparation and micro-tribological property of hydrophobic organic films on the surface of Mg–Mn–Ce magnesium alloy

Qin Liu, Zhixin Kang*

School of Mechanical and Automotive Engineering, South China University of Technology, Guangzhou 510640, China

ARTICLE INFO

Article history:
Received 5 October 2014
Received in revised form 9 January 2015
Accepted 11 February 2015

Keywords:
Organic films
Nanotribology
Adhesion
Formation mechanisium
Magnesium alloy

ABSTRACT

Two different organic compounds with a same terminal group octadecyl were used to prepare two kinds of hydrophobic organic ultrathin films on the surface of Mg–Mn–Ce alloy. The OTS film was prepared by self-assembling of the n-octadecyltrichlorosilane (OTS), and STN film was prepared by polymer-plating of another octadecyl compound 6-stearylamino-1,3,5-triazine-2,4-dithiol monosodium (STN). The surfaces were characterized by X-ray photoelectron spectroscopy (XPS), Fourier transform infrared spectroscopy (FT-IR), scanning probe microscopy, and contact angle meter. The results showed that the adhesion force at nano scale was reduced from 12.35 nN for substrate to 5.76 nN for STN film and 4.12 nN for OTS film. Besides, the nano friction force and coefficient also effectively reduced by modification of STN and OTS film on Mg–Mn–Ce alloy. Thus, hydrophobic organic films provide an effective approach to solve nano-tribological issues. Furthermore, it was also found that the differences of the friction properties between the two films were attributed to the structure of the head groups bonded to the substrate.

1. Introduction

There is a fundamental trend towards integration, miniaturization and intelligence of the instruments with the development of engineering industry [1–3]. As the lightest engineering metal material, magnesium and its alloys have attracted considerable interests due to its excellent properties, such as low density, high specific strength, good damping, electromagnetic compatibility and high dimensional stability [4]. These excellent properties of the magnesium and its alloys are very suitable for precision instruments in micro scales, such as micro electromechanical systems (MEMS) [4,5].

However, when the size of devices decreases to micro or even nano scale, because of the large surface area to volume ratio, tribological issues such as adhesion and friction would be the major reasons leading to the reduction of the performances [6,7]. Meanwhile, magnesium alloys exhibit poor wear resistance that also limits their application in the micro-scale instruments [8,9]. Herein, it will be of great significance to improve the micro tribological performances of magnesium alloys for expanding the application of magnesium alloys in micro scales.

Surface coatings have become one of the most effective methods to solve the tribological problems of magnesium alloys. Yamauchi [8] prepared diamond-like carbon (DLC) coatings on magnesium alloy surface, which were effective in decreasing the friction coefficient and improving wear resistance in both under dry conditions and in corrosive solutions. Correa [9] prepared Ni-B coatings on surface of AZ91D magnesium alloy, which also improved the tribological properties of magnesium alloy. However, many researches have found that soft lubricating coatings (polymers) are superior to the hard films in micro-tribological filed due to their self-lubricating properties, low production cost, easy to coat onto complex shapes and low shear strength [10]. Therefore, preparing organic ultrathin films as lubrication layers to improve the friction performance of the materials used in micro scales have attracted great attention [11–13]. Besides, hydrophobic surfaces are used to reduce the adhesion force and friction coefficient for their lower surface free energy compared with hydrophilic surfaces [14–16].

In this paper, two different organic compounds with a same terminal group octadecyl were used to prepare two kinds of hydrophobic organic ultrathin film on the surface of Mg–Mn–Ce alloy by self-assembling and polymer plating technology [17], respectively. The formation mechanism of the two films is studied via characterization of the surface properties. The results demonstrated that the hydrophobic organic films had a lubrication effect on friction behaviors. The distinctions of the tribological behaviors between the self-assembled film and polymer-plated film are

* Corresponding author. Tel.: +86 20 87113851; fax: +86 20 87112111.
E-mail address: zxkang@scut.edu.cn (Z. Kang).

http://dx.doi.org/10.1016/j.porgcoat.2015.02.015
0300-9440/

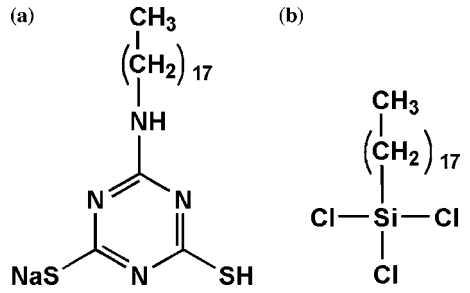

Fig. 1. Chemical structure of the two octadecyl compounds, (a) STN and (b) OTS.

compared to research the effect of film structure on tribological properties.

2. Experimental details

2.1. Materials

The Mg–Mn–Ce magnesium alloy (composition (wt.%): Mg–1.5% Mn–0.3% Ce) samples were cut into 20 mm × 20 mm × 4 mm and polished to mirror with a series of emery papers, followed by thorough ultrasonic degreasing in acetone, and then dried in cold air. The two octadecyl compounds are n-octadecyltrichlorosilane (OTS, purity 95%, Alfa Aesar) and 6-stearylamino-1,3,5-triazine-2,4-dithiol monosodium (STN, analytical reagent, Sulfur Chemical Institute Inc. of Japan). The structure of the OTS and STN are shown in Fig. 1. Deionized water (18.2 MΩ cm) was used to preparation of all aqueous solutions and for rinsing as well. Distilled water and diiodomethane (purity 99%, Alfa Aesar) were utilized to measure the contact angles. All other reagents were analytical grade and used without any further treatment.

2.2. Preparation of self-assembled monolayer

The self-assembled monolayer (SAM) solution was prepared by dissolving OTS in toluene, and the concentration was 3 mmol/L. In toluene solutions, the –Si–Cl contained in OTS monomer was hydrolyzed to –Si–OH. The pretreated Mg–Mn–Ce samples were immersed in an alkaline aqueous solution (the concentration of NaOH, Na_3PO_4 and Na_2SiO_3 was 20 g/L, 20 g/L and 25 g/L respectively) at 50 °C for 10 min to fabricate hydroxyl groups (–OH) on the surface, and immediately rinsed with distilled water, ethanol and dried in cold air. Then, the samples were soaked in OTS SAM solution for a period. The –OH on the surface would react with –Si–OH in the solution and the OTS monomers were bonded onto the surface. Afterwards, the samples were washed sequentially with distilled water and ethanol, finally dried in cold air. The prepared film was named as OTS film.

2.3. Preparation of electrochemical polymer film

The electrochemical polymer film was prepared by polymer plating [18], which was an innocuous, economic and environmental-friendly surface modification technique based on electrochemical principle [4]. The polymer-plated solution was prepared by dissolving STN monomer and sodium hydroxide (NaOH) in deionized water, and the concentration of STN and NaOH was 3 mmol/L and 0.15 mol/L respectively. A three-electrode system was used in the electrolytic cell, where Mg–Mn–Ce plate, saturated calomel electrode (SCE) and two stainless steel (SUS304) plates were used as the working electrode, the reference electrode and the counter electrode, respectively. NaOH was used as the supporting electrolyte. Galvanostatic method was utilized in process of polymer plating and the value of current density was 300 μA/cm^2. The process time was varied from 1 min to 10 min and the temperature was controlled at 20 ± 2 °C. During polymer plating, the ATP monomer would bonded to the substrate surface via electrochemical reaction. Afterwards, the sample was removed from the electrolyte and immediately rinsed with distilled water, ethanol and then dried in cold air. The prepared film was named as STN film.

2.4. Measurement

The static contact angles of distilled water and diiodomethane on the surfaces were measured by an optical contact angle meter (OCA35, Dataphysics) at ambient temperature, and a liquid droplet of 1 μl was used for contact angles measurement. The contact angle of distilled water and diiodomethane were short for WCA and DCA respectively. The average value was determined by measuring the same sample at three different positions. Fourier transform infrared (FT-IR) spectroscopy (IR Prestige-21, Shimadzu) was used to determine the chemical functional groups. X-ray photoelectron spectroscopy (XPS, AXIS Ultra, Kratos) was carried out by using a monochromatic Al *K*α X-ray source, and the binding energy was calibrated by the C 1s peak energy (284.6 eV). The surface topography and nano tribological properties were studied by scanning probe microscope system (CSPM 4000, Being Nano-instrument); the tests were performed at ambient temperature and relative humidity about 45–55%.

3. Results and discussion

3.1. Effect of the processing time on wettability of STN and OTS films

Fig. 2 shows WCA of STN film and OTS film at the different processing time. It is clearly found in Fig. 2a that the WCA of STN film increases first and then remains stable with increasing plating time. At the first 4 min of plating, electrochemical polymerization was not sufficient and the film grew with the time prolonged, which results in the WCA become larger and larger. After about 4 min of plating time, the film was completely covered on the surface and the WCA was stabled at about 132°. Similarly, the WCA of OTS film also increases firstly and then remain stable with respect to time presented in Fig. 2b. After about 2 h of self-assembling, the WCA increases to about 130°, and then the WCA remains stable at about 130–136° with the self-assembling time prolonged. Based on the influence of processing time on WCA of the two prepared films, it can be concluded that the two films were completely deposited on to the surface of Mg–Mn–Ce alloy after a period of processing time. Besides, the similar result of WCA on the surface for the two prepared films indicated that these two films with same terminal groups have a similar wettability. It is worth to mention that the processing of polymer plating was under the effect of electricity while self-assembling was a spontaneous processes, therefore, the processing time of polymer plating was shorter than self-assembling. In the following paragraphs, to ensure that the surface were covered completely by these two films, the STN film samples with a plating time 5 min and OTS film with a self-assembling time 6 h were chosen as the researched samples, respectively.

3.2. Formation mechanism of STN and OTS films

In order to confirm the chemical structure and film formation mechanism, FT-IR spectroscopy and XPS were used to analyze surface conditions. FT-IR spectra of STN film and OTS film presented in Fig. 3 displays absorption peaks about the functional groups. Compared with these two film, the absorption peaks of methyl ($-CH_3$) and methylene ($-CH_2-$) contained in octadecyl are

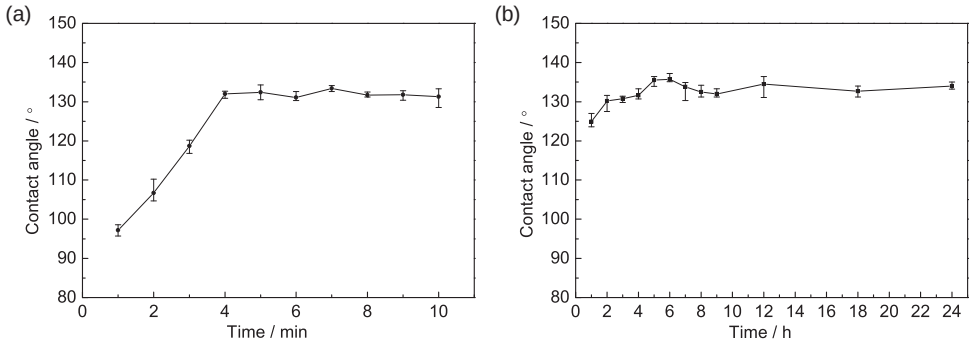

Fig. 2. Effect of the processing time on wettability of: (a) STN film and (b) OTS film.

existed in both spectra of STN and OTS films [4,19]. Peaks located at about 1440–1500 cm^{-1} are attributed to deformation vibrations of $-CH_2-$; and symmetric and asymmetric stretching vibrations of $-CH_2-$ are located at 2853 cm^{-1} and 2924 cm^{-1} respectively; peaks located at 2957 cm^{-1} are related to symmetric stretching vibrations of $-CH_3$. Besides, the peak at 1054.5 cm^{-1} is ascribed to asymmetric stretching vibrations of Si–O–Si bond that only contained in OTS film [20,21]. Similarly, peaks only presented in STN film, which located at 1547.1 and 1512.9 cm^{-1} are due to the C=N bonds related to the triazine ring contained in STN monomer [18,20]. The FT-IR spectra results suggested that the STN film and OTS film were successfully formed on Mg–Mn–Ce substrate surface.

The chemical process for the formation of the two films was researched by XPS spectra. Fig. 4 shows the wide spectra of XPS for Mg–Mn–Ce substrate and the two films. Compared to the substrate, the spectra of STN film contained N and S elements and OTS film contained Si element were detected, and the presence of lesser intensity C 1s peak on the substrate might be adsorbed from the atmosphere during handling before XPS test. The atomic concentrations of the relevant elements for XPS spectra are summarized in Table 1. It is clearly seen that the concentrations of all the original elements change a lot for the existence of the new elements contained in the two organic compounds after the processing.

The high-resolution XPS spectra for the feature elements were investigated for further confirmation of chemical structure and film formation mechanism. Fig. 5a shows the XPS spectrum of Si 2p for OTS film, and it is clearly found that Si 2p spectrum of OTS film shows three main peaks. According to the principle of electronegativity [22], the peaks located at 100.30, 100.99, 101.63 eV are assigned to Si–O–Mg, Si–O–Si, Si–O–H respectively. Si–O–Mg bonds were formed by the reaction of silanol groups (–Si–OH) contained in hydrolyzed OTS monomer and the hydroxyl (–OH) on the Mg–Mn–Ce alloy surface. The Si–O–Si bonds were formed by the mutual reaction of–Si–OH contained in OTS after hydrolysis. The Si–O–H bonds were the residues of –Si–OH after the hydrolysis of OTS monomer and were not reacted with other functional groups. Fig. 5b shows the high-resolution XPS spectrum of N 1s for STN film. Base on the research of some scholars, the binding energy of N=C and N–C would increase when they contained in a structure of ring [23,24]. Hence, the N=C and N–C contained in triazine ring of STN monomer would be located at a higher binding energy state. As a result, the binding energy at 396.68, 397.53 and 398.30 eV are related to N–H, N–C and N=C, respectively. The XPS spectrum of S 2p for STN film is displayed in Fig. 5c. It has been found that when the element sulfur is contained in the thiolate groups, two different atom specials (S 2p3/2 and S 2p1/2) are demonstrated in high-resolution XPS spectra [25,26]. The area ratio of S 2p3/2 and S 2p1/2 are 2:1, and the binding energy of S 2p3/2 is 1.2 eV lower than that of S 2p1/2. In present work, the S 2p curve is fitted as three doublets structure with the bound thiolate groups at the lowest binding energy. The binding energy of S 2p3/2 peak at 160.01 eV (S 2p1/2 at 161.21 eV) is consistent with the sulfur atoms bonded to the substrate surface as a thiolate species (S–Metal bonds, mainly refers to Mg), and the result is in agreement with previous works researched by several scholars [27,28]. The peaks at 162.02 and 163.22 eV are the S 2p3/2 peak and S 2p1/2 peak of S–S bonds which was formed by the mutual reaction of thiol groups. The peaks located at 166.57 and167.77 eV are ascribed to the oxidation of thiol groups that were not react with other groups, and the products of the oxidation were $-SO_x$ [29].

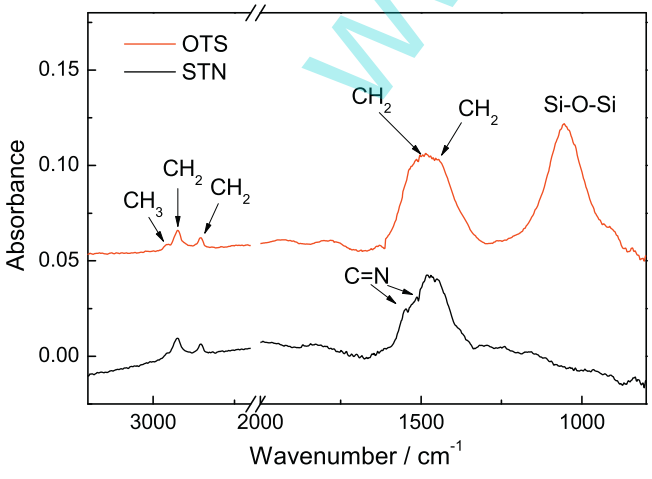

Fig. 3. FT-IR spectra of STN and OTS films on Mg–Mn–Ce surface.

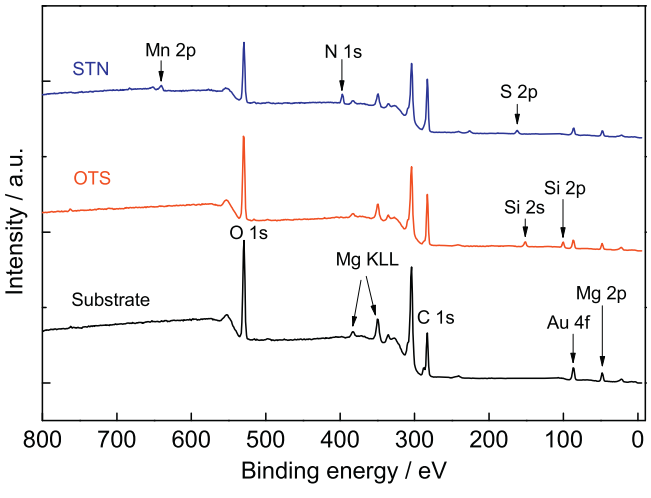

Fig. 4. XPS spectra of Mg–Mn–Ce substrate, OTS film and STN film.

Table 1
XPS atomic concentrations of the substrate, OTS and STN film (at.%).

Sample	Mg 2p	Zn 2p	C 1s	O 1s	Mn 2p	Si 2p	S 2p	N 1s
Substrate	19.82	1.40	36.86	41.92	–	–	–	–
OTS film	13.20	0.57	38.50	39.33	–	8.40		
STN film	14.54	1.25	43.60	26.87	4.98	–	3.52	5.25

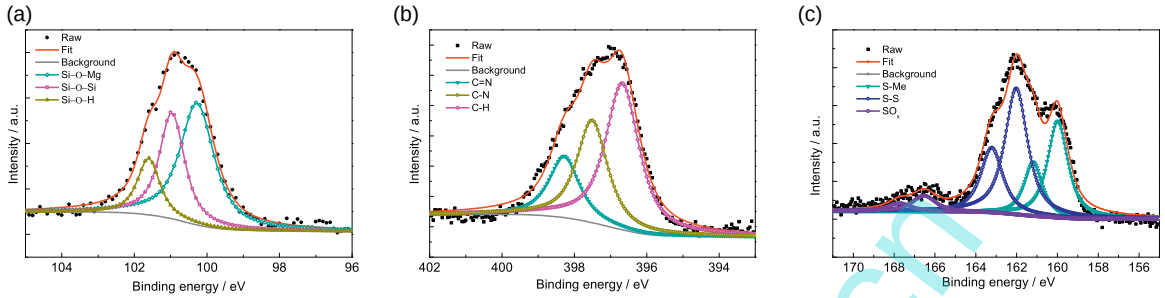

Fig. 5. High-resolution XPS spectra of (a) Si 2p for OTS film, (b) N 1s and (c) S 2p for STN film.

Based on the results of FT-IR and XPS spectra, it can be concluded that the groups contained in STN and OTS monomers were reacted with the substrate and deposited onto the substrate surface. The formation mechanism of OTS and STN films are exhibited in Fig. 6a and b respectively. The film formation of SAM (here refers to OTS film) has been reported a lot [30,31], and the process can be divided into three main steps. Firstly, silanol groups (–Si–OH) are formed by the hydrolysis of chlorosilane (–Si–Cl). Secondly, silanol groups (–Si–OH) are combined with hydroxyl (–OH) on the Mg–Mn–Ce surface or other silanol groups through hydrogen bonds. Finally, Si–O–Si bonds and Si–O–Mg are formed by dehydration condensation of hydroxyls, and the film is polymerized and covered on the surface. Similarly, the film formation of STN film is proposed as follows. DON monomer is ionized as dithiolate anions in NaOH alkaline aqueous solution, next the dithiolate anions release two electrons during electrolysis to become disulfide radicals, and then the disulfide radicals cause coupling reactions with consequent formation of the disulfide polymer, finally the disulfide polymer is coated to the conductive substrate via the effect of electrochemistry [20,32].

3.3. Characterization of OTS and STN films

Wettability and surface free energy (SFE) are important features for characterizing the variation of solid surfaces. SFE was calculated by OWRK algorithm shown in Eq. (1) with the WCA and DCA [33].

$$\frac{(1+\cos\theta)\gamma_l}{2\sqrt{\gamma_l^D}} = \sqrt{\gamma_s^P}\sqrt{\frac{\gamma_l^P}{\gamma_l^D}} + \sqrt{\gamma_s^D} \quad (1)$$

where γ_s and γ_l are the surface free energy (or surface tension) of the solid and liquid, γ^D and γ^P are the dispersion component and polar component of surface free energy (or surface tension). The results are displayed in Table 2. It can be found that after the modification of OTS film or STN film, the film has realized the transformation from a hydrophilic surface to a hydrophobic one. The SFE also changed from a higher status to a lower one. The results indicate that after modification of these two films, the hydrophobic and lower SFE functional groups $-CH_2$ and $-CH_3$ contained in octadecyl groups, are coated onto the surface. It is worth mention that the contact angles, SFE for OTS film and STN film are similar to each other, which indicates that the terminal octadecyl group has a great effect on wettability.

Fig. 7 shows the atomic force microscope (AFM) topography images of OTS film and STN film. Many polymerized clusters can be observed in both of the picture. We can clearly find that the clusters distributed on the surface of OTS film are smaller than that of STN film. Besides, the clusters in OTS film are distributed more tightly than that of STN film. The differences of the topography between these two films maybe attributed to the film formation process. OTS molecules were directly polymerized onto the substrate while STN monomers were firstly formed disulfide polymer, which formed larger clusters and then deposited onto the substrate surface, therefore, the result leads to the clusters of STN film much larger than that of OTS film.

3.4. Nano tribological properties of OTS and STN films

Tribological issues have become significant technological barriers to the successful application of durable devices at micro or even

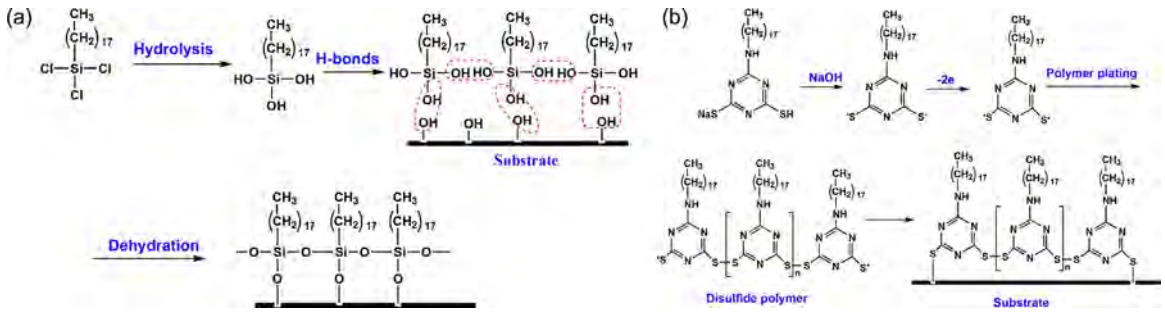

Fig. 6. Model illustration of the formation mechanism for (a) OTS film and (b) STN film.

Table 2
Contact angles and surface free energy for the substrate, STN and OTS film.

	Contact angle (°)		Surface free energy (mJ/m^2)	Dispersion	Polar
	Distilled water	Diiodomethane			
Substrate	55.0 ± 0.8	29.8 ± 2.3	51.83	37.60	14.24
STN film	132.4 ± 1.9	71.5 ± 1.3	30.81	26.09	4.72
OTS film	135.7 ± 1.5	73.9 ± 2.1	30.14	24.84	5.30

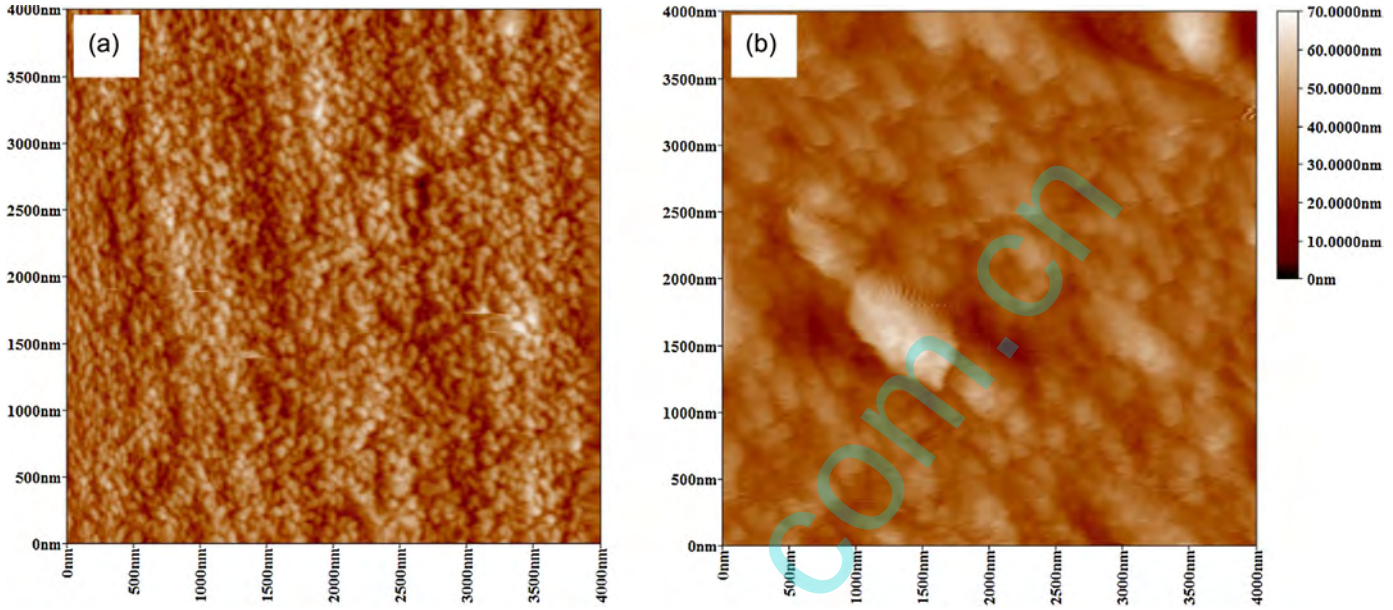

Fig. 7. AFM topography images of (a) OTS film and (b) STN film.

nano scales. Therefore, it is important to study the nano tribological properties at these small scales. In this paper, the nano tribological properties of the two films and Mg–Mn–Ce substrate were investigated by the comparison of the adhesion, friction coefficient and friction force.

3.4.1. Adhesion measurements

The adhesive force between the FFM tip and the surfaces was performed at the room temperature about 30 °C and the relative humidity about 50%. A typical force-distance curve is shown in Fig. 8 [34–36]. A → B is the probe approaching the sample surface gradually, and the cantilever of the probe does not bend. B → C is probe contacting with the sample surface suddenly due to the surface tension, and then the micro-cantilever is curved downward slightly. C → D is loading process where the degree of bending gradually increases. The probe retraces to unload when achieving the Point D, and D → F is the unloading process, where the bending degree of cantilever decreases to zero (Point E), then the cantilever bends downward gradually due to the adhesive force between the probe and the sample surface. The probe will pull off the sample surface suddenly when the adhesive force equals to the bending force of the cantilever (Point F). Finally, the probe returns to point A where no bending occurs after the probe pulling off the sample surface. The adhesive force (pull-off force) was calculated by multiplying the cantilever constant by the potential difference between points E and A shown in Eqs. (2) and (3) [37].

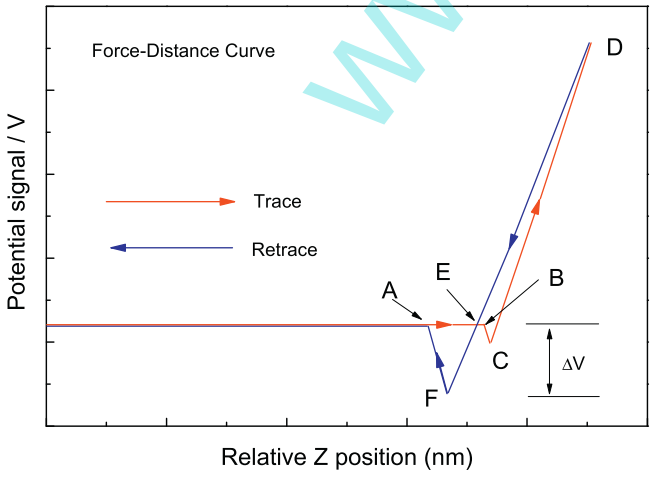

Fig. 8. A typical force-distance plot and schematic illustration for the adhesive force calculation.

$$F_{ad} = c_N S_Z \ \Delta V \tag{2}$$

$$c_N = \frac{Ewt^3}{4l^3} \tag{3}$$

where S_Z is the sensitivity of the photo detector and the value is 400.93 nm/V; c_N is the normal spring constant of the cantilever. In the test, the typical rectangular silicon cantilevers are used; E is the Young's modulus of silicon and the value is 1.69×10^{11} N/m^2. The schematic diagram of the cantilevers is shown in Fig. 9. The w, t and l are the width, thickness and length for the cantilever, respectively. It is worth mention that the l used in Eq. (3) should be the value of cantilever length minus the value of tip set back. c_N was calculated and the value is 0.2503 N/m, and Eq. (2) could be changed to Eq. (4) as follows.

$$F_{ad} = 82.31 \ \Delta V \tag{4}$$

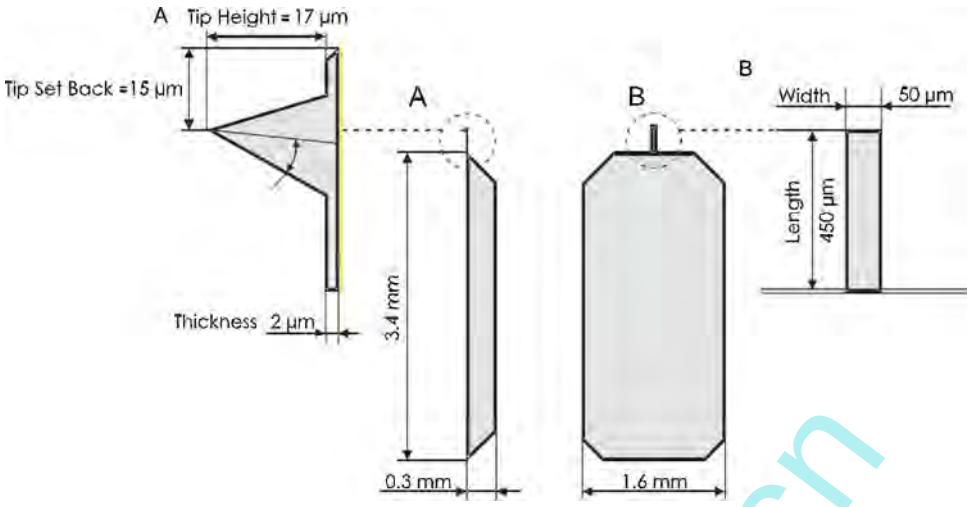

Fig. 9. Schematic diagram of a rectangular cantilever. The relevant dimensions: $l = 435$ μm, $w = 50$ μm, $t = 2$ μm, $h = 17$ μm. Note that l is given by the difference value of the cantilever length and tip set back.

Fig. 10. Model illustration of the adhesive behavior for OTS film and STN film.

The adhesion force of the substrate, STN and OTS film calculated by Eq. (4) are displayed in Table 3. It is clearly seen that the adhesion force apparently decreased when the surface was modified by STN film or OTS film. Many researchers have found that capillary condensation may occur between hydrophilic surfaces, leading to even stronger adhesive interactions [38]. The result suggests that the chemical composition of the surface have the key effect on adhesion force. The distinction of the adhesion force between STN film and OTS film surface indicates that the structure of the surface also have influence on the adhesion. According to the 3D AFM morphology, we can draw a model illustration of the adhesion behavior about the STN and OTS films shown in Fig. 10. When the tip of the probe contacted with the STN film and OTS film at a same apparent contact area, because of the smaller polymer cluster, the real contact area for OTS film is smaller than that of STN film. The attractive force between the tip and the surface are related to the real contact area, therefore, when the tip pulled off from the surface, the larger the contact area, the larger the adhesive force.

3.4.2. Nano friction properties

Nano friction force and friction coefficient also have important effect on the performance of micro scale devices. Fig. 11 shows the friction force signal of the substrate, OTS and STN film under a constant normal load signal 2 V (the normal load calculated was 16.46 nN). Similar to the adhesion results, the substrate sample showed the largest friction signal and OTS film showed the lowest friction signal. Eqs. (5) and (6) show the relationship between friction force and the friction signal [37].

$$F_L = \frac{3}{2} c_L \frac{h}{l} S_Z V_L \tag{5}$$

$$c_L = \frac{Gwt^3}{3h^2 l} \tag{6}$$

where F_L is the friction force; c_L is the lateral spring constant of the cantilever; h is the tip height; G is shear modulus of silicon cantilever and the value is 0.5×10^{11} N/m^2. It can be calculated that

Table 3
Adhesion force of Mg–Mn–Ce substrate, STN film and OTS film.

	ΔV (V)	F_{ad} (nN)
Substrate	0.15 ± 0.04	12.35 ± 3.28
STN	0.07 ± 0.02	5.76 ± 1.64
OTS	0.05 ± 0.02	4.12 ± 1.64

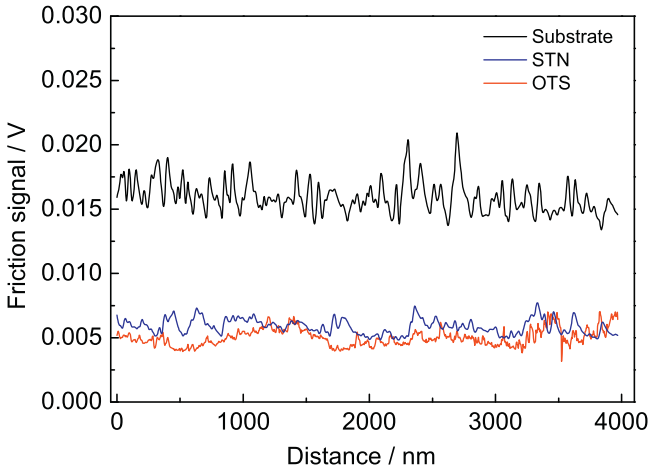

Fig. 11. Nano friction force signal of the substrate, OTS film and STN film.

Table 4
Nano friction force and coefficient of Mg–Mn–Ce substrate, STN and OTS film.

	F_L (nN)	μ
Substrate	19.82	0.454
STN film	7.30	0.094
OTS film	6.23	0.128

c_L = 53.03 N/m. Eq. (7) shows the directly proportional relationship between the friction force and friction signal.

$$F_L = 1246.35 \times V_L \quad (7)$$

Table 4 shows the friction force of the substrate and these two films. The results are in consistent with the found of many scholars that the low SFE surfaces could reduce the friction force on the surface [39,40]. After the modification of STN and OTS film, the chemical composition on the surface are $-CH_2$ and $-CH_3$, which are all lower SFE groups compared with the metal substrate, therefore, the friction force of STN and OTS film is much lower. Besides, the real contact area also affect the friction force, hence, the same as the result of adhesion test, the friction force of OTS film is also slightly lower than that of STN film.

At the small scale, the friction behavior obeys to the modified Amonton's law shown in Eq. (8) [41].

$$F_L = F_{ad} + \mu F_N \quad (8)$$

where F_L refers to friction force, F_N to applied load, F_{ad} to adhesion force, and μ to friction coefficient. Here F_N is the constant applied load 16.46 nN. The result of the friction coefficient is calculated and displayed in Table 4. The result also suggests that STN and OTS films have an effect on reducing the friction coefficient. It is worth mention that the friction coefficient of STN film is lower than that of OTS film, which is different from the results of adhesion and friction force tests. The friction coefficient is affected by both the chemical composition and the roughness, therefore, the coefficient of these two films is lower than the substrate. While for these two films, they have similar surface properties, but the roughness of STN film is lower than OTS film, therefore, the friction coefficient of STN film is lower than OTS film.

4. Conclusions

Two different organic compounds with a same terminal group octadecyl are used for the preparation of two kinds of hydrophobic organic films on the surface of Mg–Mn–Ce alloy by self-assembling and polymer plating technology, respectively. The self-assembled film was short as OTS film and polymer plated film was short as STN film. After the modification of these two films, the wettability of the Mg–Mn–Ce surface transformed from hydrophilicity to hydrophobicity. The surface free energy of OTS and STN film decreased from 51.83 mJ/m^2 for the substrate to 30.14 and 30.81 mJ/m^2, respectively.

The nano tribological properties are evaluated by friction force microscope. The adhesion and friction force, friction coefficients were all reduced by both OTS and STN films in comparison with the Mg–Mn–Ce substrate. It is demonstrated that the surface properties like wettability and surface free energy have a great effect on reducing adhesion force and improving friction properties. Besides, based on the comparison of the tribological properties between STN film and OTS film, it can be concluded that surface structure (topography) like roughness also has an important effect on the friction properties. Therefore, designing a special surface structure on a lower SFE surface is an effective approach to solving tribological issues for magnesium alloys.

Acknowledgments

This work is supported by the National Natural Science Foundation of China (no. 51075151) and Key Program of Guangdong Natural Science Foundation (no. 10251064101000001).

References

[1] M. Teodorescu, S. Theodossiades, H. Rahnejat, Impact dynamics of rough and surface protected MEMS gears, Tribol. Int. 42 (2009) 197–205.
[2] B. Bhushan, Nanotribology and nanomechanics of MEMS/NEMS and BioMEMS/BioNEMS materials and devices, Microelectron. Eng. 84 (2007) 387–412.
[3] V.K. Goel, L. Ferrara, Basic science symposium II: MEMS technology, SAS J. 2 (2008) 120–129.
[4] Z.X. Kang, X.M. Lai, J. Sang, Y.Y. Li, Fabrication of hydrophobic/superhydrophobic nanofilms on magnesium alloys by polymer plating, Thin Solid Films 520 (2011) 800–806.
[5] L.M. Jiang, Z.Y. Cheng, N. Du, W. Li, Z.Q. Tian, Z.W. Tian, Electrochemical micromachining microstructure lattice on magnesium alloy surface, Acta Phys. Chim. Sin. 24 (2008) 1307–1312.
[6] N. Satyanarayana, S.K. Sinha, L. Shen, Effect of molecular structure on friction and wear of polymer thin films deposited on Si surface, Tribol. Lett. 28 (2007) 71–80.
[7] Z.X. Kang, Q. Liu, Y.H. Liu, Preparation and micro-tribological property of hydrophilic self-assembled monolayer on single crystal silicon surface, Wear 303 (2013) 297–301.
[8] N. Yamauchi, K. Demizu, N. Ueda, N.K. Cuong, T. Sone, Y. Hirose, Friction and wear of DLC films on magnesium alloy, Surf. Coat. Technol. 193 (2005) 277–282.
[9] E. Correa, A.A. Zuleta, L. Guerra, M.A. Gómez, J.G. Castaño, F. Echeverría, H. Liu, P. Skeldon, G.E. Thompson, Tribological behavior of electroless Ni-B coatings on magnesium and AZ91D alloy, Wear 305 (2013) 115–123.
[10] B. Bhushan, A.V. Kulkarni, V.N. Koinkar, M. Boehm, L. Odoni, C. Martelet, M. Belin, Microtribological characterization of self-assembled and Langmuir-Blodgett monolayers by atomic and friction force microscopy, Langmuir 11 (1995) 3189–3198.
[11] P.H. Suegama, A.A.C. Recco, A.P. Tschiptschin, I.V. Aoki, Influence of silica nanoparticles added to an organosilane film on carbon steel electrochemical and tribological behaviou, Prog. Org. Coat. 60 (2007) 90–98.
[12] N. Satyanarayana, S.K. Sinha, Tribology of PFPE overcoated self-assembled monolayers deposited on Si surface, J. Phys. D: Appl. Phys. 38 (2005) 3512–3522.
[13] Y.B. Guo, D.G. Wang, S.H. Liu, S.W. Zhang, Fabrication and tribological properties of polyelectrolyte multilayers containing in situ gold and silver nanoparticles, Colloids Surf. A 417 (2013) 1–9.
[14] B. Bhushan, H.W. Liu, S.M. Hsu, Adhesion and friction studies of silicon and hydrophobic and low friction films and investigation of scale effects, J. Tribol. 126 (2004) 583–590.
[15] M. Jin, X. Feng, J. Xi, J. Zhai, K. Cho, L. Feng, L. Jiang, Super-hydrophobic PDMS surface with ultra-low adhesive force, Macromol. Rapid. Commun. 26 (2005) 1805–1809.
[16] S.L. Ren, S.R. Yang, Y.P. Zhao, Nano-tribological study on a super-hydrophobic film formed on rough aluminium substrates, Acta Mech. Sin. 20 (2004) 159–164.
[17] Z.X. Kang, Q. Ye, J. Sang, Y.Y. Li, Fabrication of super-hydrophobic surface on copper surface by polymer plating, J. Mater. Process. Technol. 209 (2009) 4543–4547.
[18] K. Mori, H. Hirahara, Y. Oishi, N. Kumagai, Polymer plating of 2-dioctylamino-1,3,5-triazine-4,6-dithiol to magnesium alloys, Electrochem. Solid-State Lett. 3 (2000) 546–549.
[19] X. Cui, S. Zhong, H. Wang, Synthesis and characterization of emulsifier-free core-shell fluorine-containing polyacrylate latex, Colloids Surf. A 303 (2007) 173–178.
[20] Q. Liu, Z.X. Kang, G. Fang, Preparation and properties of polymeric nano composite film on surface of sintered NdFeB permanent magnet, Acta Phys. Chim. Sin. 29 (2013) 821–828.
[21] M.T. Kim, Deposition behavior of hexamethydisiloxane films based on the FTIR analysis of Si–O–Si and Si–CH_3 bonds, Thin Solid Films 311 (1997) 157–163.
[22] J.G. Liao, X.J. Wang, Y. Zuo, L. Zhang, J.Q. Wen, Y.B. Li, Surface modification of nano-hydroxyapatite with silane agent, J. Inorg. Mater. 23 (2008) 145–149.
[23] T. Ujvári, A. Kolitsch, A. Tóth, M. Mohai, I. Bertóti, XPS characterization of the composition and bonding states of elements in CN_x layers prepared by ion beam assisted deposition, Diam. Relat. Mater. 11 (2002) 1149–1152.
[24] S. Souto, M. Pickholz, M.C. Dos Santos, F. Alvarez, Electronic structure of nitrogen-carbon alloys (a-CN_x) determined by photoelectron spectroscopy, Phys. Rev. B 57 (1998) 2536–2540.
[25] D.G. Castner, K. Hinds, D.W. Grainger, X-ray photoelectron spectroscopy sulfur 2p study of organic thiol and disulfide binding interactions with gold surfaces, Langmuir 12 (1996) 5083–5086.
[26] Y.H. Liu, Z.X. Kang, Preparation and characterization of a polymeric dielectric film with a low surface free energy, Acta Phys. Chim. Sin. 27 (2011) 1777–1782.
[27] G. Panzmer, B. Egert, The bonding state of sulfur segregated to α-iron surfaces and on iron sulfide surfaces studied by XPS, AES and ELS, Surf. Sci. 144 (1984) 651–664.

[28] M. Descostes, F. Mercier, N. Thromat, C. Beaucaire, M. Gautier-Soyer, Use of XPS in the determination of chemical environment and oxidation state of iron and sulfur samples: constitution of a data basis in binding energies for Fe and S reference compounds and applications to the evidence of surface species of an oxidized pyrite in a carbonate medium, Appl. Surf. Sci. 165 (2000) 288–302.
[29] J.A. Rodriguez, J. Hrbek, J. Dvorak, T. Jirsak, A. Maiti, Interaction of sulfur with TiO_2 (110): photoemission and density-functional studies, Chem. Phys. Lett. 336 (2001) 377–384.
[30] A. Ulman, Formation and structure of self-assembled monolayers, Chem. Rev. 96 (1996) 1533–1554.
[31] J. Choi, T. Ishida, T. Kato, S. Fujisawa, Self-assembled monolayer on diamond-like carbon surface: formation and friction measurements, Tribol. Int. 36 (2003) 285–290.
[32] K. Mori, Y. Sasaki, S. Sai, S. Kaneda, H. Hirahara, Y. Oishi, Electrochemical polymerization of 2-(dioctylamino)-1,3,5-triazine-4,6-dithiol on iron plates, Langmuir 11 (1995) 1431–1434.
[33] M. Gindl, G. Sinn, W. Gindl, A. Reiterer, S. Tschegg, A comparison of different methods to calculate the surface free energy of wood using contact angle measurements, Colloids Surf. A 181 (2001) 279–287.
[34] X. Li, W. Guan, H. Yan, L. Huang, Fabrication and atomic force microscopy/friction force microscopy (AFM/FFM) studies of polyacrylamide-carbon nanotubes (PAM-CNTs) copolymer thin films, Mater. Chem. Phys. 88 (2004) 53–58.
[35] Y. Guo, D. Wang, S. Liu, Tribological behavior of in situ Ag nanoparticles/polyelectrolyte composite molecular deposition films, Appl. Surf. Sci. 256 (2010) 1714–1719.
[36] Y.B. Guo, D.G. Wang, S.W. Zhang, Adhesion and friction of nanoparticles/polyelectrolyte multilayer films by AFM and micro-tribometer, Tribol. Int. 44 (2011) 906–915.
[37] B. Bhushan, Springer Handbook of Nanotechnology, 3rd ed., Springer-Verlag Berlin Heidelberg, 2010.
[38] S.P. Pujari, E. Spruijt, M.A. Cohen Stuart, C.J.M. van Rijn, J.M.J. Paulusse, H. Zuilhof, Ultralow adhesion and friction of fluoro-hydro alkyne-derived self-assembled monolayers on H-terminated Si (111), Langmuir 28 (2012) 17690–17700.
[39] B. Bhushan, T. Kasai, G. Kulik, L. Barbieri, P. Hoffmann, AFM study of perfluoroalkylsilane and alkylsilane self-assembled monolayers for anti-stiction in MEMS/NEMS, Ultramicroscopy 105 (2005) 176–188.
[40] Y. Song, R. Premachandran Nair, M. Zou, Y.A. Wang, Adhesion and friction properties of micro/nano-engineered superhydrophobic/hydrophobic surfaces, Thin Solid Films 518 (2010) 3801–3807.
[41] G.B. Yang, X.H. Chen, K.D. Ma, L.G. Yu, P.Y. Zhang, The tribological behavior of spin-assisted layer-by-layer assembled Cu nanoparticles-doped hydrophobic polyelectrolyte multilayers modified with fluoroalkylsilane, Surf. Coat. Technol. 205 (2011) 3365–3371.